IOPscience iopscience.iop.org

Home Search Collections Journals About Contact us My IOPscience

Electronic structures of ReS_2, $ReSe_2$ and TcS_2 in the real and the hypothetical undistorted structures

This article has been downloaded from IOPscience. Please scroll down to see the full text article.

1997 J. Phys.: Condens. Matter 9 4411

(http://iopscience.iop.org/0953-8984/9/21/008)

View the table of contents for this issue, or go to the journal homepage for more

Download details:
IP Address: 171.66.16.207
The article was downloaded on 14/05/2010 at 08:47

Please note that terms and conditions apply.

J. Phys.: Condens. Matter **9** (1997) 4411–4424. Printed in the UK PII: S0953-8984(97)82112-1

Electronic structures of ReS_2, $ReSe_2$ and TcS_2 in the real and the hypothetical undistorted structures

C M Fang, G A Wiegers, C Haas and R A de Groot

Chemical Physics, Materials Science Centre, University of Groningen, Nijenborg 4, 9747 AG Groningen, The Netherlands

Received 24 February 1997

Abstract. The transition-metal dichalcogenides ReX_2 (X = S or Se) and TcS_2 with a d^3 electron configuration have distorted $CdCl_2$ and $Cd(OH)_2$ structures, respectively, with the Re(Tc) atoms in each layer forming parallelogram-shaped connected clusters (diamond chain). *Ab-initio* band-structure calculations were performed for ReX_2 and TcS_2, and the hypothetical undistorted 1T-TcS_2 and 3R-ReX_2 structures. The calculations show that ReS_2, $ReSe_2$ and TcS_2 are semiconductors with energy gaps of about 1.0 eV, 0.5 eV and 0.7 eV, respectively, while for the undistorted structures the Fermi level is in the partly filled band of $d_{x^2-y^2}$ and d_{xy} orbitals of the t_{2g} manifold.

X-ray photoemission spectra for the core levels and valence band of $ReSe_2$ and ReS_2 are presented. The valence x-ray photoemission spectra showed that ReS_2 is a p-type semiconductor with an energy gap of about 1.5 eV, while $ReSe_2$ is an n-type semiconductor. The experimental results are in good agreement with the band-structure calculations.

1. Introduction

The Tc and Re disulphides and selenides have a layered structure and semiconducting properties like the Mo and W dichalcogenides [1, 2]. However, the origin of the semiconductivity is different. For the Mo and W dichalcogenides which have a d^2 electron configuration and trigonal-prismatic coordination of the metal atoms by chalcogen atoms, there is a low-lying d_{z^2} band of the metal which is completely occupied by two electrons [1, 3]. For the group VII dichalcogenides which have a d^3 electron configuration the origin of the semiconductivity is a distortion of a $Cd(OH)_2$- or $CdCl_2$-type basic structure to a structure with metal–metal bonds in parallelogram-shaped clusters along one of the in-plane axes (diamond chain). The transition can be simply thought to take place as follows: the metal atoms form zigzag chains in which two of the three d electrons are used in metal–metal bonds, followed by a Peierls distortion along the chain, leading to four-atom parallelogram-shaped clusters. In this MO scheme all d electrons are paired.

Because of their layered structure and easy cleavage parallel to the layers, STM and AFM surface studies can easily be performed [4–6]. In contrast with the transition-metal dichalcogenides such as 1T-TiS_2 and 2H-MoS_2, the chalcogen top layer and the subsurface Re layers of ReX_2 have different geometries, and STM and AFM of these compounds may show the contributions of the top chalcogen layers and the subsurface metal atoms to the images, depending on the parameters of the measurements. Such measurements have been reported by several workers, but with conflicting results and interpretations [4–9].

Structural information on the Re and Tc dichalcogenides was based on the crystal structure determination of $ReSe_2$ by Alcock and Kjekshus [10] and unit-cell dimensions

0953-8984/97/214411+14$19.50 © 1997 IOP Publishing Ltd

and structures proposed on the basis of that of $ReSe_2$ by Wildervanck and Jellinek [2] for ReS_2, $ReSe_2$, ReSSe, TcS_2 and $TcSe_2$. Wildervanck and Jellinek showed that ReS_2, $ReSe_2$ and ReSSe have a triclinic distorted $CdCl_2$ structure with in-plane axes twice those of the hypothetical undistorted structure, while TcS_2 has a similar distorted $Cd(OH)_2$-type structure. Recently Lamfers *et al* [11] reported the x-ray single-crystal structure determinations of $ReSe_2$, ReS_2, ReSSe and TcS_2 using crystals grown by Wildervanck and Jellinek [2]. Lamfers *et al* [11] showed that the structure of $ReSe_2$ as determined by Alcock and Kjekshus is wrong in the sense that these workers interchanged inversion centres and pseudo-inversion centres. Four-atom clusters of Re atoms are present, but the Re–Re and the Re–Se distances differ strongly from those of Alcock and Kjekshus. Unit-cell dimensions and the structure of ReS_2 determined by Lamfers *et al* [11] differ from those published recently by Murray *et al* [12] in the sense that a doubled *c* axis was found. Diamond chains similar to those of $ReSe_2$ are present. TcS_2 has a distorted $Cd(OH)_2$-type structure with a Tc diamond chain.

Optical measurements showed energy gaps of about 1.32 eV, 1.17 eV and 1.3 eV for ReS_2, $ReSe_2$ and TcS_2 [1, 13–15], respectively. The compounds may have application in thin-film solar cells [16], in electrochemical solar cells [17], and as catalysts for sulphur-tolerant hydrogenation and hydrosulphurization [18, 19]. Recently their use as a polarization-sensitive detector for light was reported [20].

The electronic structures of ReS_2 and $ReSe_2$ were studied by Kertesz and Hoffmann [21] and by Whangbo and co-workers [5, 22–25] in the course of their study on the origin of the lattice distortions in transition-metal dichalcogenides with d^n electron count ($n = 1$, 2, 3) using extended Hückel tight-binding band-structure calculations [26]. Kertesz and Hoffmann [21] concluded that a Jahn–Teller distortion is responsible for the particular pattern of clustering in $ReSe_2$. Whangbo and co-workers [22–25] explained the diamond chains in these d^3 compounds in terms of hidden 1D Fermi surfaces of the undistorted structures.

Until now no *ab-initio* band-structure calculation and photoemission spectra were reported for the Tc and Re dichalcogenides. In this paper we describe band-structure calculations using the localized-spherical-wave (LSW) method, with the structural data from Lamfers *et al* [11] as input. In order to recognize the driving force for the distortion the band structures of the hypothetical undistorted structures (1T-TcS_2, 3R-ReS_2 and 3R-$ReSe_2$) were also calculated. The chemical bonding and structural distortions are discussed in connection with the calculated band structures. X-ray photoemission spectra for the core levels and the valence bands of ReS_2 and $ReSe_2$ were measured. The calculated results are compared with the experimental data.

2. Structure of ReS_2, $ReSe_2$ and TcS_2

The crystal data determined by Lamfers *et al* [11] are listed in table 1; the space group is $P\bar{1}$. The axes are chosen such that *a* and *b* are the in-plane axes; the chains with clusters of metal atoms are along the shortest of the two, i.e. the *a* axis. The unit cells of $ReSe_2$ and TcS_2 contain one sandwich; ReS_2 with a doubled *c* axis contains two sandwiches related by symmetry centres. For the discussion of the structural characteristics and the band-structure calculations of ReS_2 we take a structure with only one sandwich per unit cell (*c* halved and the centre of symmetry in the Re layers). Now we have in all three cases two crystallographically independent metal atoms (M(1) and M(2)) and four crystallographically independent X (X = S or Se) atoms (X(1), X(2), X(3) and X(4)) for all the compounds numbered in the same way. The metal atoms form chains of connected clusters of four M atoms along the *a* axes as shown in figure 1. The M atoms in the clusters are related by

inversion centres; the shortest metal–metal distance is for the central bond of the cluster between the M(2) atoms related by the inversion centre at 1/2, 1/2, 1/2. The M–M distances in the cluster of figure 2 are given in table 2. The M atoms are in distorted octahedra of chalcogen atoms; the six independent M–X distances differ considerably, but the averages are about the same for the two independent metal atoms (2.392 Å, 2.396 Å and 2.521 Å for TcS_2, ReS_2 and $ReSe_2$, respectively). The X(1) and X(2) atoms are inside the space above the rows of M atoms forming the cluster chain. X(3) and X(4) are between adjacent chains. X(1) and X(2) are at a larger distance from the plane $z = \frac{1}{2}$ (approximately the plain of the metal atoms) than the X(3) and X(4) atoms (table 3). Each X atom is coordinated approximately trigonal-pyramidally to three M atoms. The average X–M distances vary in the sequence X(4) > X(3) > X(2) > X(1); those for $ReSe_2$ are given in table 3. The X layers are much more distorted from hexagonal symmetry than found by Alcock and Kjekshus [10] for $ReSe_2$ The Se–Se distances along rows of Se, e.g. parallel to [100], show an alternation in length of about 10%. For the [100] direction, one row consists of alternate Se(1) and Se(2) with distances of 3.417 and 3.219 Å, and the adjacent rows of alternate Se(3) and Se(4) with distances of 3.455 and 3.163 Å. The rows deviate somewhat from linearity, e.g. the angles Se(1)–Se(2)–Se(1) and Se(3)–Se(4)–Se(3) are 167.6° and 170.9° respectively. Approximately the same structural features are found for ReS_2 and TcS_2.

Table 1. Unit-cell dimensions of TcS_2, ReS_2 and $ReSe_2$. Z is the number of formula units per cell. a and b are the in-plane axes; the chains of metal clusters are along the a axis. The space group is $P\bar{1}$.

	a (Å)	b (Å)	c (Å)	α (deg)	β (deg)	γ (deg)	Z
TcS_2	6.371	6.464	6.654	62.94	103.61	119.00	4
ReS_2	6.352	6.446	12.779	91.51	105.17	118.97	8
$ReSe_2$	6.597	6.710	6.721	91.84	104.90	118.91	4

Table 2. Metal–metal distances in the diamond chain of $ReSe_2$, ReS_2 and TcS_2. The numbering of the distances refers to figure 2.

	M–M distance (Å)		
	$ReSe_2$	ReS_2	TcS_2
1–2	2.871	2.808	2.817
$1–2_i$	2.844	2.785	2.788
$2–2_i$	2.733	2.693	2.700
$1–1_{ia}$	2.987	2.881	2.8981
$2–1_a$	3.734	3.551	3.562

The hypothetical undistorted structures are of the $Cd(OH)_2$ type, space group $P\bar{3}m1$, for 1T-TcS_2 and of the $CdCl_2$ type, space group $R\bar{3}m$, for ReS_2 and $ReSe_2$. The unit-cell dimensions of the undistorted structures in table 4 are obtained with the assumption that the distortion causes a doubling of the in-plane dimensions of the unit cell of the undistorted structure and no change in the distance between neighbouring sandwiches. The ratio c/a (c taken for one sandwich) is as high as 1.90, which means that the metal atoms are in trigonal elongated octahedra of chalcogen atoms as for example in 1T-VSe_2. The Re–S, Re–Se and Tc–S distances, calculated with $z = 0.25$ for S and Se, are also listed in table 4. The metal–metal distances are equal to the length of the a axis.

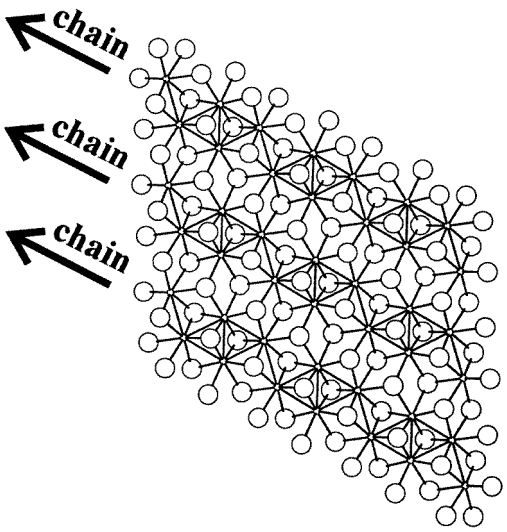

Figure 1. The basal plane of $ReSe_2$ with chains of Re clusters along [100] as a prototype for all three compounds. The large circles represent Se atoms, and the small circles Re atoms.

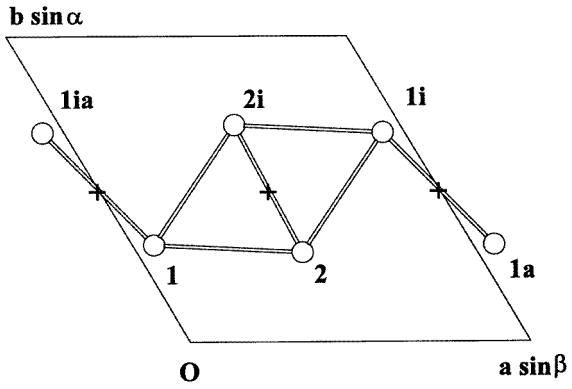

Figure 2. Projection of the metal cluster chain along the stacking axis c. Inversion centres are indicated by $+$. The distances between the numbered atoms are given in table 2. Note that the X atoms X(1) and X(2) at $z = 3/4$ project inside the triangles $2–2_i–1_i$ and $1–1_{ia}–1_i$, respectively. X(3) and X(4) project between chains.

3. Band-structure calculations

3.1. Calculation method

Ab initio band-structure calculations were performed with the LSW [27] method using a scalar-relativistic Hamiltonian. We used local-density exchange–correlation potentials [28] inside space filling, and therefore overlapping spheres around the atomic constituents. The self-consistent calculations were carried out including all core electrons.

Iterations were performed with $\boldsymbol{k}$ points distributed uniformly in the irreducible part of the first Brillouin zone (BZ), corresponding to a volume of the BZ per $\boldsymbol{k}$ point of the

Table 3. The coordinate z, the height above the plane $z = 1/2$ and the selenium–rhenium bond distances for Se(1), Se(2), Se(3) and Se(4) of $ReSe_2$.

	Se(1)		Se(2)		Se(3)		Se(4)
z	0.793 86		0.761 32		0.723 66		0.696 64
Height (Å)	1.876		1.668		1.429		1.255
Re(2) (Å)	2.472	Re(1)	2.534	Re(1)	2.494	Re(1)	2.582
Re(1) (Å)	2.469	Re(1)	2.433	Re(2)	2.494	Re(2)	2.574
Re(2) (Å)	2.466	Re(2)	2.531	Re(1)	2.623	Re(2)	2.591
Average (Å)	2.476	Average	2.496	Average	2.537	Average	2.582

Table 4. Space groups, unit-cell dimensions, the ratios c/a per sandwich, Z (the number of formula units per cell) and the M–X bond distances of the hypothetical undistorted structures 1T-TcS_2, 3R-ReS_2 and 3R-$ReSe_2$; the M–X distance is calculated with the z coordinate of S and Se equal to 0.25.

Compound	Space group	a (Å)	c (Å)	Z	c/a	M–X distance (Å)
1T-TcS_2	$P\bar{3}m1$	3.209	5.924	1	1.846	2.372
3R-ReS_2	$R\bar{3}m$	3.200	18.194	3	1.895	2.390
3R-$ReSe_2$	$R\bar{3}m$	3.327	19.018	3	1.905	2.490

Table 5. Input parameters of atoms (Re, Se; Tc, S) and empty spheres (Va) for the band-structure calculations of 3R-ReX_2 (X = S or Se) and 1T-TcS_2, and the output of the electronic configurations. R_{WS} represents the Wigner–Seitz radius.

Atom		x	y	z	R_{WS} (Å)	Electronic configuration
1T-TcS_2						
Tc	1a	0	0	0	1.1623	[Kr] $4d^{4.75}5s^{0.16}5p^{0.20}4f^{0.03}$
S	2d	1/3	2/3	1/4	1.6789	[Ne] $3s^{1.91}3p^{4.56}3d^{0.29}$
Va	1b	0	0	1/2	1.1623	$1s^{0.11}2p^{0.15}3d^{0.09}$
3R-ReS_2						
Re	3a	0	0	0	1.1695	[Xe] $5d^{4.42}6s^{0.21}6p^{0.20}5f^{0.03}$
S	6c	0	0	1/4	1.6892	[Ne] $3s^{1.91}3p^{4.63}3d^{0.37}$
Va	3b	0	0	1/2	1.1695	$1s^{0.11}2p^{0.13}3d^{0.09}$
3R-$ReSe_2$						
Re	3a	0	0	0	1.2302	[Xe] $5d^{4.56}6s^{0.27}6p^{0.23}5f^{0.03}$
Se	6c	0	0	1/4	1.7535	[Ar] $4s^{1.91}4p^{4.13}4d^{0.52}4f^{0.22}$
Va	3b	0	0	1/2	1.2302	$1s^{0.11}2p^{0.13}3d^{0.08}$

order of 3×10^{-5} Å^{-3}. Self-consistency was assumed when the changes in the local partial charges in each atomic sphere decreased to the order of 10^{-5}.

In the construction of the LSW basis [27, 29], the spherical waves were augmented by solutions of the scalar-relativistic radial equations labelled by the following atomic symbols: 3s, 3p and 3d; 4s, 4p and 4d; 5s, 5p and 4d; 6s, 6s and 5d. These correspond to the valence levels of the elements S, Se, Tc and Re, respectively. External l summation, which is used to augment a Hankel function at surrounding atoms, was extended to $l = 3$, resulting in the use of 4f orbitals for Se, Tc and Re. When the crystal is not very densely packed,

as in the case of the layered compounds, it is necessary to include empty spheres in the calculations. The empty spheres are located at the octahedral site in the van der Waals gaps. The functions 1s and 2p, and 3d as an extension, were used for empty spheres.

3.2. Electronic structure of hypothetical 1T-TcS_2 and 3R-ReX_2 (X = S or Se)

Table 5 lists the input parameters (unit-cell dimensions, atomic positions and Wigner–Seitz radii) and calculated electronic configurations of the atoms for 1T-TcS_2 and for 3R-ReX_2 (X = S or Se). We remark that not too much significance should be attributed to the orbital configuration in table 5, as these numbers depend strongly on the Wigner–Seitz radii and the presence of empty spheres. Part of the d orbital occupation is due to hybridization contribution of d orbitals in occupied s or p orbitals.

The BZs for 1T-TcS_2 and 3R-ReX_2 are shown in figures 3 and 4, respectively. Partial and total density of states (DOS), as well as the dispersion of the energy bands, are shown in figures 5–7. Energies, dominant orbital characters (OC) and symmetries at point Γ of the BZ are listed in table 6.

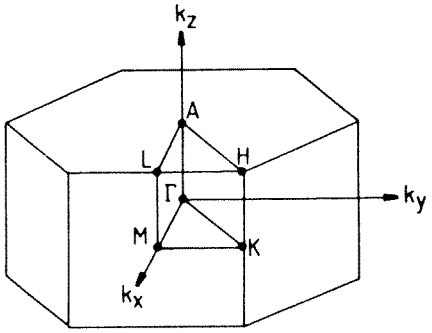

Figure 3. BZ and high-symmetry points for 1T-TcS_2.

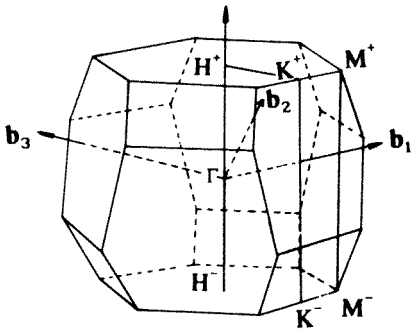

Figure 4. BZ and high-symmetry points for 3R-ReX_2.

The calculated band structures of 1T-TcS_2 and 3R-ReX_2 are very similar owing to the trigonal-antiprismatic coordination of the metal atoms by chalcogen atoms. The band structures are composed of three main bands separated by energy gaps. The lowest band consist of two S 3s or Se 4s bands; the next six bands are mainly S 3p or Se 4p hybridized with Tc 4d or Re 5d. Three Tc 4d (Re 5d) orbitals form a non-bonding t_{2g} band with d_{z^2} at the bottom and $d_{x^2-y^2}$ and d_{xy} at the top of the band. The d_{z^2} orbital is the lowest because of the large c/a ratio (note that the z axis is perpendicular to the layers). The next two bands form the antibonding e_g manifold of the transition metal. The crystal-field splitting between the t_{2g} and the e_g band is easily seen.

1T-TcS_2 and 3R-ReX_2 are metallic with three electrons in the d states of the transition-metal atoms. Two of the three electrons are in the Tc 4d (Re 5d) orbitals strongly hybridized with the chalcogen p states. The bands show a broad dispersion over all the valence bands. One d (Tc 4d or Re 5d) electron is in the two orbitals at the upper part of the valence band. These two orbitals are mainly $d_{x^2-y^2}$ and d_{xy} of Re or Tc hybridized with some p_x and p_y orbitals of the chalcogen atoms; they have a small dispersion and are therefore quite localized (with a band width of about 1.3 eV).

According to the dispersion of the energy bands, the Fermi surfaces for the undistorted structures 1T-TcS_2 and 3R-ReX_2 can be mapped out. The structures of the Fermi surfaces

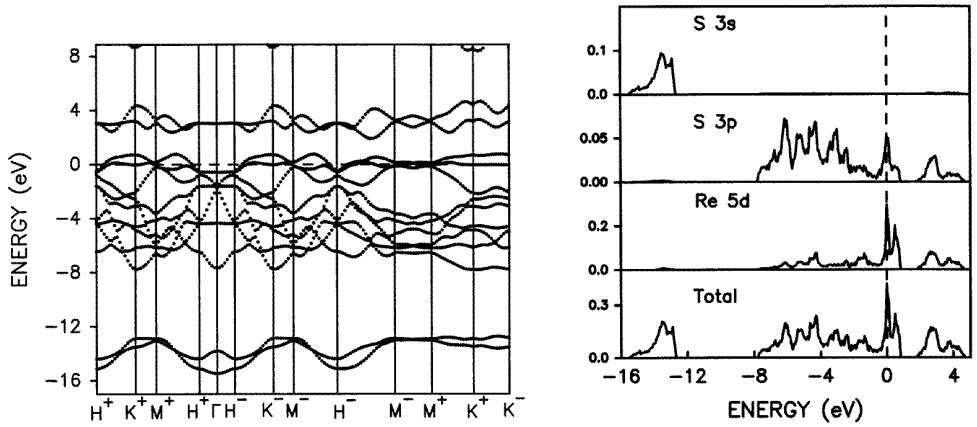

(a) (b)

Figure 5. (a) Dispersion of the energy bands and (b) partial and total DOSs for 3R-ReS_2.

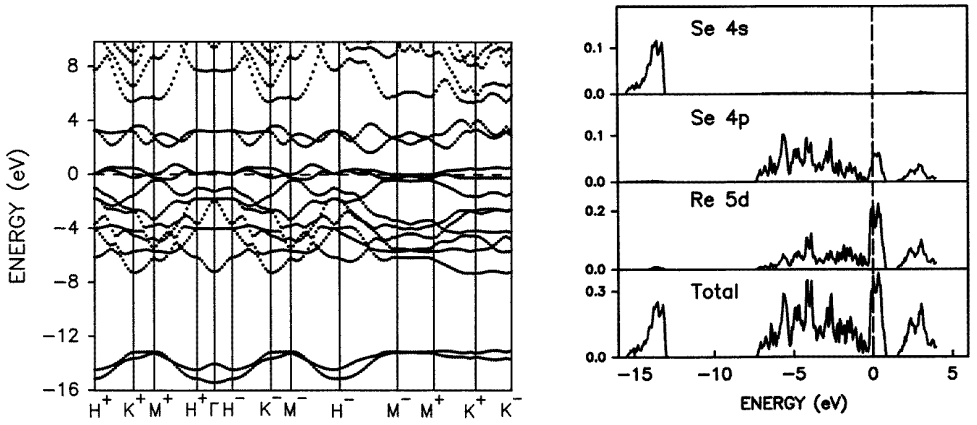

(a) (b)

Figure 6. (a) Dispersion of the energy bands and (b) partial and total DOSs for 3R-$ReSe_2$.

of the three hypothetical compounds are quite different. The Fermi surfaces for 1T-TcS_2 and 3R-ReS_2 are complex. For TcS_2 there are two cylinders around Γ–A, six cylinders around M–L, and six ellipsoids around H, which are all occupied by electrons. For 3R-ReS_2 there are two cylinders along H–Γ and 12 ellipsoids around the M points, which are occupied by electrons. For 3R-$ReSe_2$ the Γ–H cylinders are unoccupied.

The Fermi surfaces for the three hypothetical structure are quite three dimensional. The calculations show that S $3p_z$ (Se $4p_z$) bands have a dispersion of 2–3 eV and that the interactions in the interlayer direction are strong, although the net interaction across the van der Waals gap is weak. It is well known that Fermi surface nesting is the driving force for small distortions of the structure. Therefore 2D models such as (hidden) Fermi surface nesting leading to doubling of the *a* and *b* axes, as proposed by Whangbo and co-workers [22–25] as the origin of the distortion, is just a first-order approximation and not sufficient to describe the large distortions observed in the Re and Tc dichalcogenides.

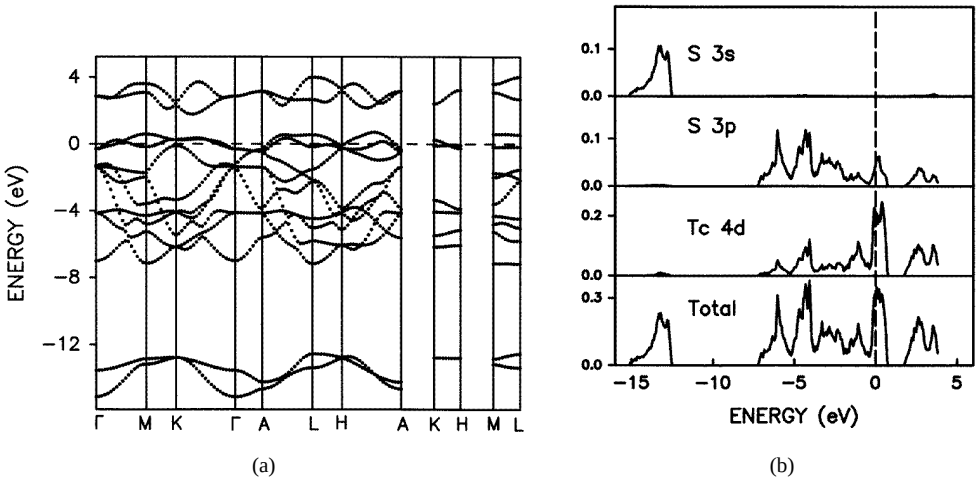

(a) (b)

Figure 7. (a) Dispersion of the energy bands and (b) partial and total DOSs for 1T-TcS_2.

At the Fermi level the DOS is very high. In combination with electron–phonon interactions, this results in an instability of the undistorted crystal structure. The calculations show that two of the three d electrons are strongly hybridized with the p_x and p_y orbitals of the chalcogen atoms, and there is only one electron in the two localized $d_{x^2-y^2}$ and d_{xy} orbitals of the transition-metal atoms. The transition is therefore expected to affect the in-plane structure of the transition-metal atoms. The hexagonal layers of S (Se) limit deformation too far from the original structure, and the $d_{x^2-y^2}$ and d_{xy} states will remain approximately degenerate. Overlap of the $d_{x^2-y^2}$ and d_{xy} orbitals of neighbouring metal atoms, filling the orbitals with four electrons and opening a gap, is possible when a four-atom cluster is formed. The only reasonable geometry to bring four transition atoms together on a hexagonal plane is a diamond chain.

3.3. Electronic structures of TcS_2 and ReX_2

The input parameters for the band-structure calculations are given in table 7. The partial and total DOSs in figures 8–10 show that the compounds are semiconductors.

For TcS_2 the S 3s band ranges from −15.2 to −12.4 eV when the Fermi level is set at the bottom of the conduction band, compared with from −15.2 to −12.5 eV for 1T-TcS_2. For the different S atoms the S 3s states have different characteristic peaks, because of the different coordinations by Tc atoms (similar to that for $ReSe_2$ in table 3). The valence band, consisting of S 3p hybridized with Tc 4d states, begins at −7.25 eV and ends at −0.7 eV. The energy gap is therefore 0.7 eV. A clear t_{2g}–e_g splitting of the octahedral crystal field as seen in the undistorted structure is no longer visible. The calculations show that the conduction band is mainly composed of Tc 4d orbitals mixed with some S 3p states. The top of the valence band and the bottom of the conduction band are at the Γ point. The DOS of TcS_2 has S 3s and S 3p states similar to those of the undistorted structure because the Tc–S bonds do not change much in the two structures.

The DOSs for ReS_2 and $ReSe_2$ are quite similar to that of TcS_2 (figures 8–10). For $ReSe_2$ the Se 4s band has a width of 2.7 eV (from −15.4 to −12.7 eV with respect to the Fermi level at the bottom of the conduction band), similar to that of 3R-$ReSe_2$. The valence band from −7.3 to −0.5 eV consists of mainly Se 4p hybridized with Re 5d states.

Table 6. Energies, dominant OCs and symmetry (according to Miller and Love [13]) of the states at Γ for 3R-ReX_2 and 1T-TcS_2 nd* indicates a mix of $n\mathrm{d}_{x^2-y^2}$, $n\mathrm{d}_{xy}$, $n\mathrm{d}_{xz}$ and $n\mathrm{d}_{yz}$ orbitals.

3R-ReS_2			3R-$ReSe_2$			1T-TcS_2		
E (eV)	Symmetry	OC	E (eV)	Symmetry	OC	E (eV)	Symmetry	OC
−15.47	1+	S 3s	−15.48	1+	Se 4s	−15.13	1+	S 3s
−13.79	2−	S 3s	−14.06	2−	Se 4s	−13.55	2−	S 3s
−7.68	1+	S $3p_z$	−7.19	1+	Se $4p_z$	−7.00	1+	S $3p_z$
−4.35	3+	S $3p_xp_y$	−3.99	3+	Re 5d*	−4.12	3+	Tc 4d*
−1.81	2−	S $3p_z$	−1.89	1+	Re $5d_{z^2}$	−1.38	3+	S $3p_xp_y$
−1.69	1+	Re $5d_{z^2}$	−1.75	3+	Se $4p_xp_y$	−1.34	1+	Tc $4d_{z^2}$
−1.60	3+	Re 5d*	−1.27	2−	Se $4p_z$	−1.32	2−	S $3p_z$
−0.57	3−	S $3p_xp_y$	+0.14	3−	Se $4p_xp_y$	−0.39	3−	S $3p_xp_y$
3.03	3+	Re 5d*	3.12	3+	Re 5d*	2.85	3+	Tc 3d*

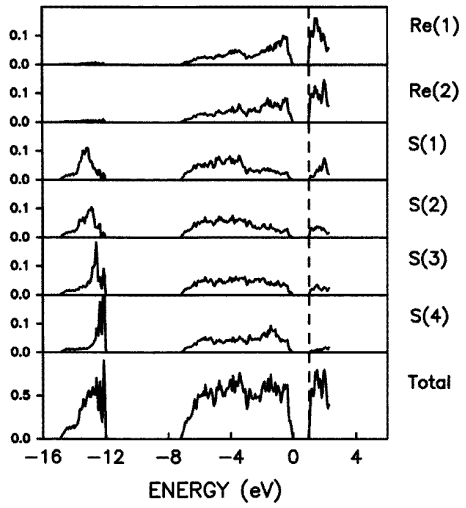

Figure 8. Partial and total DOSs for ReS_2.

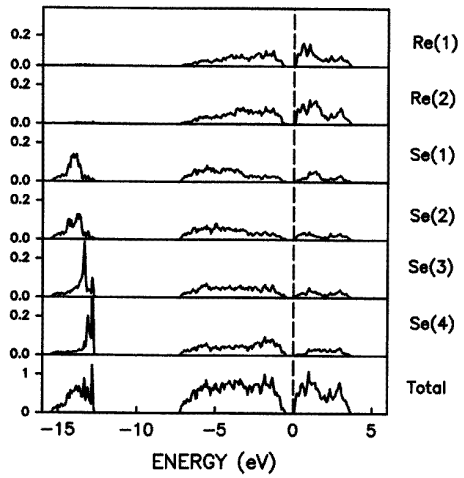

Figure 9. Partial and total DOSs for $ReSe_2$.

The bottom of the conduction band is composed mainly of Re 5d states mixed with a small amount of Se 4p orbitals. $ReSe_2$ is therefore a semiconductor with an energy gap of about 0.5 eV. The calculations show that neither the top of the valence band nor the bottom of the conduction band is at the Γ point, and the direct energy gap at Γ is about 1.1 eV.

For ReS_2 the S 3s band ranges from −15.9 to −13.0 eV with respect to the Fermi level at the bottom of the conduction band. The valence band has a width of 7.2 eV (from −8.2 to −1.0 eV). There is an energy gap of about 1.0 eV between the valence and the conduction band. Kelty *et al* [5] obtained a band gap of 1.27 eV for a single ReS_2 layer and 0.81 eV for the bulk from the calculations.

It is remarkable that the DOSs of the valence bands of ReX_2 and TcS_2 have a very broad and flat shape, in contrast with those of hypothetical 1T-TcS_2 and 3R-ReX_2. In the real structures all the three d electrons are dispersive over the whole valence band and are strongly hybridized with S 3p (Se 4p) states. This is a consequence of a stronger overlap

Table 7. Input parameters of atoms (Tc, Re, Se, S) and empty spheres (Va) and the output of electronic configurations. R_{WS} represents the Wigner–Seitz radius.

Atom	x	y	z	R_{WS} (Å)	Electronic configuration
TcS_2					
Tc(1)	0.939 67	0.693 58	0.490 41	1.141	[Kr] $4d^{4.75}5s^{0.15}5p^{0.18}4f^{0.02}$
Tc(2)	0.489 53	0.285 05	0.502 85	1.141	[Kr] $4d^{4.74}5s^{0.15}5p^{0.18}4f^{0.02}$
S(1)	0.3611	0.3076	0.7900	1.648	[Ne] $3s^{1.90}3p^{4.50}3d^{0.29}$
S(2)	0.8240	0.2802	0.7622	1.623	[Ne] $3s^{1.89}3p^{4.40}3d^{0.23}$
S(3)	0.1434	0.1714	0.2741	1.699	[Ne] $3s^{1.92}3p^{4.60}3d^{0.30}$
S(4)	0.3211	0.8124	0.7011	1.759	[Ne] $3s^{1.93}3p^{4.80}3d^{0.33}$
Va(1)	0.0000	0.0000	0.0000	1.105	$1s^{0.10}2\ p^{0.12}3d^{0.06}$
Va(2)	0.8610	0.6100	0.0700	0.801	$1s^{0.06}2\ p^{0.04}3d^{0.01}$
Va(3)	0.3400	0.1050	0.1260	0.771	$1s^{0.07}2\ p^{0.04}3d^{0.01}$
Va(4)	0.5000	0.5000	0.0000	0.821	$1s^{0.06}2\ p^{0.04}3d^{0.01}$
Va(5)	0.5000	0.0000	0.0000	1.131	$1s^{0.11}2\ p^{0.13}3d^{0.07}$
Va(6)	0.0000	0.5000	0.0000	1.141	$1s^{0.09}2\ p^{0.11}3d^{0.06}$
ReS_2					
Re(1)	0.9432	0.690 35	0.5080	1.121	[Xe] $5d^{4.31}6s^{0.18}\ 6p^{0.16}5f^{0.03}$
Re(2)	0.5119	0.7144	0.5020	1.141	[Xe] $5d^{4.40}6s^{0.21}6\ p^{0.19}5f^{0.03}$
S(1)	0.7486	0.6164	0.7858	1.695	[Ne] $3s^{1.92}3p^{4.63}3d^{0.42}$
S(2)	0.2758	0.6563	0.7574	1.695	[Ne] $3s^{1.91}3p^{4.65}3d^{0.38}$
S(3)	0.7723	0.8898	0.2761	1.695	[Ne] $3s^{1.91}3p^{4.71}3d^{0.34}$
S(4)	0.2462	0.8651	0.3023	1.695	[Ne] $3s^{1.91}3p^{4.77}3d^{0.31}$
Va(1)	0.0000	0.0000	0.0000	1.131	$1s^{0.07}2p^{0.09}3d^{0.06}$
Va(2)	0.8800	0.6500	0.1150	0.763	$1s^{0.07}2p^{0.04}3d^{0.01}$
Va(3)	0.3300	0.1000	0.0680	0.912	$1s^{0.07}2p^{0.06}3d^{0.02}$
Va(4)	0.5000	0.5000	0.0000	1.022	$1s^{0.08}2p^{0.08}3d^{0.04}$
Va(5)	0.5000	0.0000	0.0000	1.047	$1s^{0.06}2p^{0.06}3d^{0.04}$
Va(6)	0.0000	0.5000	0.0000	1.022	$1s^{0.07}2p^{0.07}3d^{0.03}$
$ReSe_2$					
Re(1)	0.936 85	0.685 23	0.508 62	1.224	[Xe] $5d^{4.58}6s^{0.28}6p^{0.23}5f^{0.03}$
Re(2)	0.487 23	0.290 42	0.496 81	1.224	[Xe] $5d^{4.58}6s^{0.29}6p^{0.24}5f^{0.03}$
Se(1)	0.751 84	0.618 08	0.793 86	1.720	[Ar] $4s^{1.91}4p^{4.02}4d^{0.49}4f^{0.24}$
Se(2)	0.720 49	0.339 02	0.238 68	1.693	[Ar] $4s^{1.90}4p^{4.02}4d^{0.43}4f^{0.19}$
Se(3)	0.226 10	0.108 62	0.723 66	1.769	[Ar] $4s^{1.92}4p^{4.16}4d^{0.49}4f^{0.24}$
Se(4)	0.245 04	0.863 54	0.303 36	1.845	[Ar] $4s^{1.94}4p^{4.39}4d^{0.54}4f^{0.28}$
Va(1)	0.835 66	0.151 18	0.058 66	0.968	$1s^{0.07}2p^{0.06}3d^{0.02}$
Va(2)	0.000 00	0.000 00	0.000 00	1.137	$1s^{0.07}2p^{0.07}3d^{0.04}$
Va(3)	0.500 00	0.500 00	0.000 00	1.077	$1s^{0.08}2p^{0.08}3d^{0.04}$
Va(4)	0.500 00	0.000 00	0.000 00	1.034	$1s^{0.06}2p^{0.05}3d^{0.02}$
Va(5)	0.000 00	0.500 00	0.000 00	1.050	$1s^{0.07}2p^{0.06}3d^{0.03}$
Va(6)	0.396 56	0.680 00	0.081 64	0.789	$1s^{0.06}2p^{0.04}3d^{0.01}$

of the wavefunctions of Tc 4d (Re 5d) orbitals owing to the shorter Tc–Tc (or Re–Re) distances.

The calculations show near the top of the valence band higher S 3p (Se 4p) DOSs for X(3) and X(4) than for X(1) and X(2), whereas at greater distance from the top the partial DOSs are higher for X(1) and X(2). This is a consequence of the changes in the chalcogen-to-metal distances X(4) > X(3) > X(2) > X(1). At the bottom of the conduction band the Tc 4d (Re 5d) orbitals have a much higher DOS (about four times) than S 3p (Se 4p), indicating that the conduction band is mainly 4d or 5d of the transition metal.

The band-structure calculations performed for ReS_2 and $ReSe_2$ here are difficult to

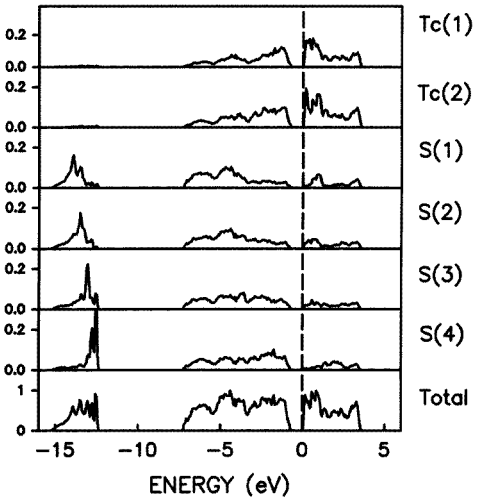

Figure 10. Partial and total DOSs for 1T-TcS_2.

compare with the calculations by Whangbo and co-workers [5, 9]. These workers present only DOS curves for a single slab in order to understand STM data. In addition their calculations are semiempirical.

4. X-ray photoemission spectra

The crystals were grown by Wildervanck and Jellinek [2]. The crystals used were approximately squares with rounded sides, with dimensions of about 5–10 mm. X-ray photoelectron spectroscopy measurements were carried out in a small-spot ESCA machine from VG. A spot size of 300–600 μm was used. The radiation source was an Al anode using the Kα line with a photon energy of 1486.6 eV. The sample surface was cleaned by stripping with Scotch tape in the preparation chamber at a base pressure of 10^{-9} Torr. The sample with a fresh surface was transported to the main chamber (base pressure, 10^{-10} Torr).

The wide range of x-ray photoelectron spectra of $ReSe_2$ and ReS_2 showed hardly any contamination by oxygen and carbon. The x-ray photoelectron spectra of the core levels are consistent with those in the literature for the elements [30] with consideration of chemical shifts, except for a higher-energy difference between ReS_2 and $ReSe_2$ due to the Fermi level difference (ReS_2 is an n-type semiconductor; see below, where it is stated that $ReSe_2$ grown with I_2 as transport agent is a p-type semiconductor). Figure 11 shows the x-ray photoelectron spectra of the Re 4f core level electrons for ReS_2 and $ReSe_2$. The peak splittings (Re $4f_{7/2}$ and $4d_{5/2}$) and peak widths are the same for ReS_2 and $ReSe_2$; the binding energies for ReS_2 are shifted by about 1.0 eV to a higher energy owing to the Fermi level shift. This indicates that the Re atoms have the same valence in $ReSe_2$ and ReS_2.

The x-ray photoelectron spectra of the valence bands for ReS_2 and $ReSe_2$ are shown in figure 12. The S 3s band of ReS_2 has a width of about 5.0 eV (from -17.5 to -12.5 eV). The valence band of ReS_2 (from -9.0 to about -1.0 eV) shows an energy gap of about 1 eV below the Fermi level, which means that ReS_2 is an n-type semiconductor with a gap

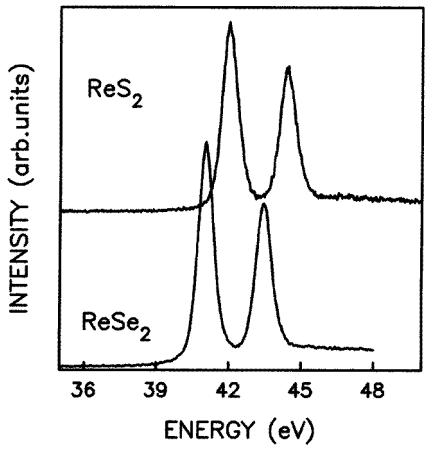

Figure 11. X-ray photoemission spectra of the 4f core levels of ReS_2 and $ReSe_2$.

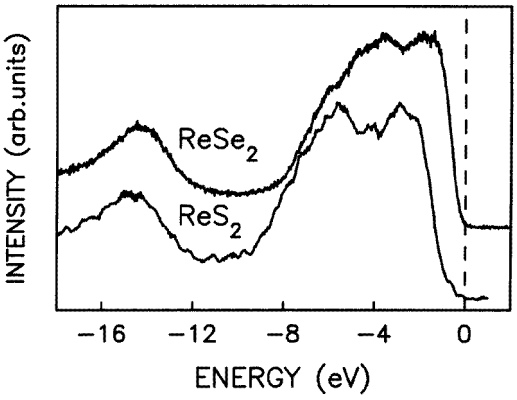

Figure 12. X-ray photoemission spectra of the valence bands of ReS_2 and $ReSe_2$.

of about 1.0 eV, corresponding well to the energy gap of 1.32 eV deduced from the optical absorption spectra [2, 13–15]. The Se 4s band of $ReSe_2$ ranges from −17.0 to −12.0 eV. The valence band begins from about −8.0 eV to the Fermi level. The Fermi level is at the top of the valence band which confirms the p-type semiconductivity observed in transport measurements. Figure 13 and 14 show the x-ray photoelectron spectra of the valence band of ReS_2 and $ReSe_2$ and the spectrum calculated using the cross sections for photoemissions [31]. For comparison the spectra are shifted to a lower energy of about 1.6 eV and 0.6 eV for ReS_2 and $ReSe_2$, respectively. If the spectra resolution (about 1.0 eV for photons with an energy of 1486.6 eV) is taken into consideration, the calculated spectra are in good agreement with the measurements.

5. Conclusions

Using the *ab-initio* LSW method the electronic structures for ReS_2, $ReSe_2$ and TcS_2, and their undistorted structures 3R-ReS_2, 3R-$ReSe_2$ and 1T-TcS_2, are reported. The undistorted

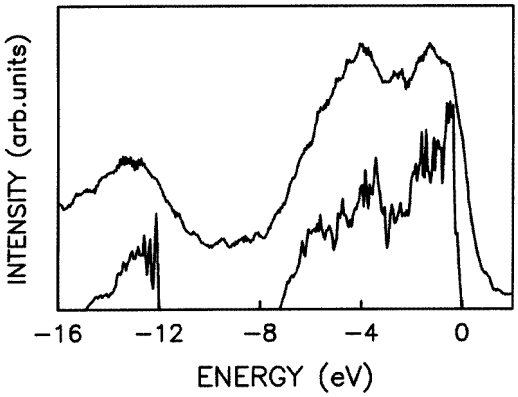

Figure 13. X-ray photoemission spectrum of the valence band of ReS_2 and the calculated spectrum.

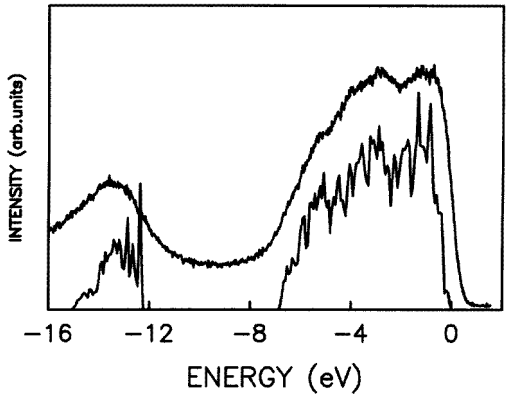

Figure 14. X-ray photoemission spectrum of the valence band of $ReSe_2$ and the calculated spectrum.

structures have a trigonal-antiprismatic crystal-field splitting in the band structures. The Fermi level is in the $d_{x^2-y^2}$ and d_{xy} part of the t_{2g} manifold and contains one electron; the d_{z^2} orbital is hybridized with chalcogen p and lies at a lower energy.

ReS_2, $ReSe_2$ and TcS_2 are semiconductors with energy gaps of about 1.0, 0.5 and 0.7 eV, respectively.

Photoelectron spectra for the core level and valence band of ReS_2 and $ReSe_2$ were obtained. The valence band spectra of ReS_2 and $ReSe_2$ are in good agreement with the band-structure calculations.

Acknowledgment

We thank Dr H-J Lamfers for providing information on his crystal structure determination prior to publication and some figures.

References

[1] Wilson J A, DiSalvo F J and Mahajan S 1975 *Adv. Phys.* **24** 117
[2] Wildervanck J C and Jellinek F 1971 *J. Less-Common Met.* **24** 73
[3] Doni E and Girlanda R 1986 *Electronic Structure and Electronic Transitions in Layered Materials* ed V Grasso (Dordrecht: Reidel)
[4] Friemelt K, Akari S, Lux-Steiner M-Ch, Schill T, Bucher E and Dransfeld K 1992 *Ann. Phys., Lpz.* **1** 248
[5] Kelty S P, Ruppert A F, Chianelli R R, Ren J and Whangbo M-H 1994 *J. Am. Chem. Soc.* **116** 7857
[6] Lloyd D R 1993 *Ann. Phys., Lpz.* **2** 755
[7] Friemelt K, Akari S, Lux-Steiner M-Ch, Schill T, Bucher E and Dransfeld K 1993 *Ann. Phys., Lpz.* **2** 758
[8] Ren J and Whangbo M-H 1992 *Phys. Rev.* B **46** 4917
[9] Parkinson B A, Ren J and Whangbo M-H 1991 *J. Am. Chem. Soc.* **113** 7833
[10] Alcock N W and Kjekshus A 1965 *Acta Chem. Scand.* **19** 79
[11] Lamfers H-J, Meetsma A, Wiegers G A and de Boer J L 1996 *J. Alloys Compounds* **241** 34
[12] Murray H H, Kelly S P, Chianelli R R and Day C S 1994 *Inorg. Chem.* **33** 4418
[13] Leicht G, Berger H and Levy F 1987 *Solid State Commun.* **61** 531
[14] Marzik J V, Kershaw R, Dwight K and Wold A 1984 *J. Solid State Chem.* **51** 170
[15] Friemelt K, Kulikova L, Kulyuk L, Siminel A, Arushanov E, Kloc Ch and Bucher E 1996 *J. Appl. Phys.* **79** 9268
[16] Aruchamy A 1992 *Physics and Chemistry of Materials with Low-dimensional Structure* (Dordrecht: Kluwer)
[17] Wheeler B L, Leland J K and Bard A J 1986 *J. Electrochem. Soc.* **133** 358
[18] McNicol B D 1977 *J. Catal.* **46** 438
[19] Lacoix M, Boutarfa N, Guillard C, Vrinat M and Bresse M 1989 *J. Catal.* **120** 473
[20] Friemelt K, Lux Steiner M-Ch and Bucher E 1993 *J. Appl. Phys.* **74** 5266
[21] Kertesz M and Hoffmann R 1984 *J. Am. Chem. Soc.* **106** 3453
[22] Whangbo M-H and Canadell E 1992 *J. Am. Chem. Soc.* **114** 9587
[23] Rovira C and Whangbo M-H 1993 *Inorg. Chem.* **32** 4097
[24] Whangbo M-H, Seo D-K and Canadell E 1996 *Physics and Chemistry of Low-Dimensional Inorganic Conductors* ed C Schlenker, J Dumas, M Greenblatt and S van Smaalen (New York: Plenum) p 285
[25] Whangbo M-H, Canadell E, Foury P and Pouget J P 1991 *Science* **252** 96
[26] Whangbo M-H and Hoffmann R 1978 *J. Am. Chem. Soc.* **100** 6093
[27] van Leuken H, Lodder A, Czyzyk M T, Springelkamp F and de Groot R A 1990 *Phys. Rev.* B **41** 5613
[28] Hedin L and Lundqvist B I 1971 *J. Phys. C: Solid State Phys.* **4** 2064
[29] Anderson O K and Jepsen O 1984 *Phys. Rev. Lett.* **53** 2571
[30] Wagner C D, Riggs W M, Davis L E, Moulder J F and Muilenberg G E 1978 *Handbook of X-ray Photoelectron Spectroscopy* (Eden Prairie, MN: Perkin–Elmer)
[31] Yeh J J and Lindau Yu I 1985 *At. Data and Nucl. Data Tables* **32** 1